JACS Au
AN OPEN ACCESS JOURNAL OF THE AMERICAN CHEMICAL SOCIETY

pubs.acs.org/jacsau
Article

Surface Hydration of Porous Nickel Hydroxides Facilitates the Reversible Adsorption of CO_2 from Ambient Air

Xiaowei Wu, Rahul Pandey, Junyan Zhang, Felipe Polo-Garzon, Fransisco Carlos Robles Hernandez, Ramanan Krishnamoorti, and Praveen Bollini*

Cite This: JACS Au 2025, 5, 1649−1662
Read Online
ACCESS | Metrics & More | Article Recommendations | Supporting Information

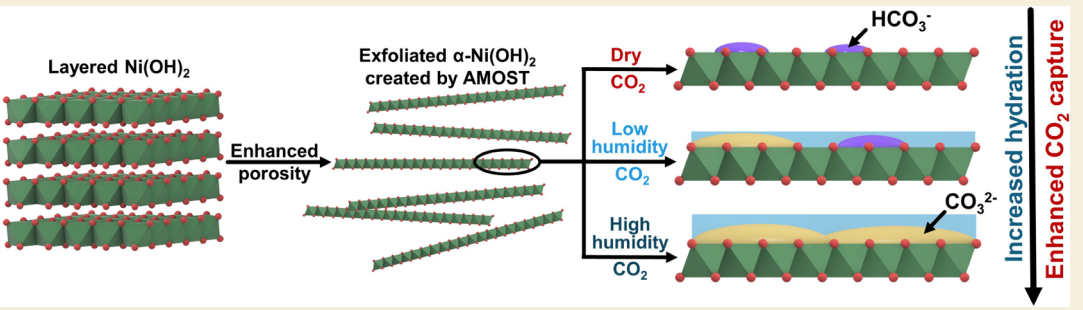

ABSTRACT: Direct air capture (DAC) under humid ambient conditions typically requires the use of organic components, with sorbents that are purely inorganic in composition for the most part operating hundreds of degrees above room temperature. In this work, we report porous metal hydroxides as a novel class of water-tolerant, oxidatively and hydrothermally stable low-temperature sorbents that exhibit competitive DAC working capacities of 1.25 mmol/g over 5 consecutive temperature swing adsorption−desorption cycles in the presence of steam and oxygen. Aqueous miscible organic solvent treatments are used to create highly porous structures with surface areas exceeding 700 m^2/g that capture CO_2 in the form of bicarbonates under dry conditions, and carbonates under wet conditions. Water exerts a facilitative rather than an inhibiting effect on CO_2 binding, and the presence of hydrating multilayers serves to stabilize carbonate species—akin to moisture swing adsorbents—except for the fact that solvation results in a remarkable (upto 10-fold) increase, not decrease, in DAC capacity. High-valent doping with cerium is used to improve DAC capacities by amplifying surface basicity, evidencing porous nickel hydroxides specifically (and porous metal hydroxides more generally) as a novel class of robust, earth-abundant DAC sorbents.

KEYWORDS: *CO_2 capture, layered double hydroxides, solvation, temperature swing adsorption, porous metal hydroxides*

1. INTRODUCTION

Climate change mitigation remains the defining challenge facing mankind in the 21st century. There is growing consensus that reversing the already calamitous trends in anthropogenic CO_2 emissions is predicated on the use of negative emission technologies that extract CO_2 directly out of the atmosphere.[1,2] Over and above reversing emissions trends, the intentional removal of CO_2 from air using direct air capture (DAC) technologies also helps address adverse effects of distributed sources that account for up to two-thirds of global CO_2 emissions.[3] Temperature swing adsorption (TSA) processes are highly attractive for DAC due in part to the fact that they apply work to concentrated CO_2 rather than the dilute feed containing only 400 ppm of carbon dioxide.[4] A variety of solid sorbent materials have been evaluated in this context, including zeolites, metal−organic frameworks (MOFs), supported amines, and bulk metal oxides. Each of these existing classes of sorbent materials, however, suffers from specific limitations that encumber their practical use. Zeolites, for instance, although hydrothermally stable, are highly unselective to CO_2 in the presence of water vapor.[5,6] MOF physisorbents exhibit similar challenges with competitive water adsorption.[6,7] Dehumidification of air streams can resolve such selectivity limitations, but likely result in heavy energy inputs;[5,8] even MOFs that do appear to be CO_2 selective in the presence of water can in fact exhibit non-negligible losses in adsorption capacity in the presence of water vapor.[9] Hybrid organic−inorganic sorbents such as MOFs and supported amines exhibit limited stability in the presence of oxygen, with the latter also suffering from leaching of organics that oftentimes degrades DAC performance over time.[7,10]

Received: November 13, 2024
Revised: February 11, 2025
Accepted: February 13, 2025
Published: March 17, 2025

Scheme 1. (a) Illustration of the Layered Double Hydroxide (LDH) Structure; (b) Depiction of LDH Delamination by Aqueous Miscible Organic Solvent Treatment (AMOST), Adapted with permission from Ref 26, Copyright 2013 Royal Society of Chemistry; and (c) Illustration of α-Ni(OH)$_2$ and β-Ni(OH)$_2$ Crystal Structures, Reprinted with Permission from Ref 29, Copyright 2020 Springer Nature.

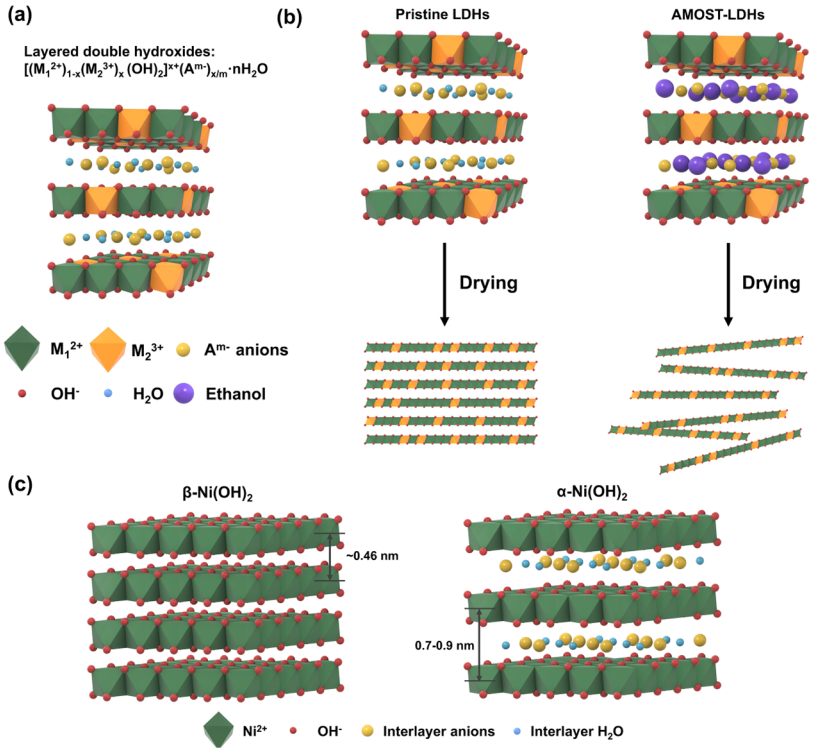

Mitigation of stability issues in supported amine sorbents through the use of alternative capture moieties such as secondary amines and polyamines with longer spacers lends promise from a lifetime standpoint, but can result in lower CO_2 adsorption capacities.[11−13] These modifications could also increase sorbent manufacturing costs due to the limited commercial availability of alternative polyamines, combined with the additional steps that their complex synthesis protocols entail.

Calcium and magnesium oxides are the most commonly investigated oxide-based CO_2 capture sorbents. These oxides are relatively inexpensive compared to supported amine systems and possess high theoretical CO_2 adsorption capacities that can exceed values of 15 mmol CO_2 per gram of sorbent.[14,15] CO_2 forms strongly bound carbonates on these sorbents, however, requiring temperatures in excess of 400 °C for their conversion back to oxides.[16,17] These sorbents are also hampered by slow adsorption kinetics resulting from diffusion limitations, as demonstrated in the literature. Rausis et al., for instance, reported slow carbonation kinetics under DAC conditions for MgO, with only 16 wt % of the sorbent being carbonated in an entire year.[18] CaO sorbents can also be limited by adsorption kinetics; a stream of 500 ppm of CO_2 at temperatures as high as 300 °C still requires 100 min for 35 wt % carbonation.[19] Alkaline-earth metal oxides therefore appear to not be viable low-temperature DAC sorbents due to the lack of sizable working capacities under ambient conditions.

More generally, to the best of our knowledge, no purely inorganic DAC sorbent has been reported to date that treats humid ambient air streams at reasonable time scales. This, despite the fact that hydroxide groups in other classes of materials such as MOFs have been shown to capture CO_2 at low temperatures. Dong et al., for instance, attributed the reasonable DAC capacity of MOF-808—0.21 mmol CO_2/g at 25 °C—to the formation of intramolecular hydrogen bonds between neighboring Zr−OH sites.[20] The Wade and Ho groups reported DAC capacities greater than 2 mmol/g at 27 °C over benzotriazolate MOFs bearing Ni/Zn-hydroxyls.[21,22] These prior studies support the feasibility of using hydroxyl groups for low-temperature DAC applications specifically, and the potential use of surface hydroxyls ubiquitous on bulk (hydr)oxide surfaces for CO_2 capture more generally. Our own group previously reported the interaction of CO_2 formed in situ under catalytic ethane oxidation conditions with unsupported NiO samples prepared using a solid-state decomposition procedure.[23] Multiple types of carbonate species with highly distinct binding characteristics were formed on these NiO surfaces, pointing to the tunability of the CO_2 binding using bulk Ni oxides as a platform. As reflected in their highly tunable and hydrothermally stable structure, bulk oxides and hydroxides are, in principle, more ideal carriers of oxygen-containing nucleophiles for DAC applications compared to MOF materials that tend to inherently be more susceptible to degradation.[24]

Surface area limitations of (hydr)oxide powders can potentially be overcome through the use of layered double hydroxides (LDHs)—a class of highly tunable metal hydroxides that carry the requisite porosity for DAC applications and that are characterized by a two-dimensional structure comprised of cationic metal hydroxide and charge-balancing anion interlayers (Scheme 1a).[25] We demonstrate herein the first example of the use of LDH-derived solid sorbents to deliver competitive DAC equilibrium and working adsorption capacities, oxidative and hydrothermal stability,

https://doi.org/10.1021/jacsau.4c01083
JACS Au 2025, 5, 1649−1662

recyclability, water tolerance, and CO_2 selectivity. We use aqueous miscible organic solvent treatment (AMOST) protocols developed by O'Hare and coworkers[26] to synthesize high surface area hydroxides with the requisite gravimetric adsorption site density, and use doping with high-valent metals to accentuate the nucleophilicity of (hydr)oxide active sites toward CO_2 adsorption. Hydroxide groups that adsorb CO_2 in these materials exhibit much stronger tolerance to oxidation compared with nitrogen moieties in supported amine sorbents, likely due to the fact that unlike organic−inorganic hybrid materials, the adsorbing functional group in the material reported is itself inherently rich in oxygen.[27] α-polymorphs of nickel hydroxides reported here represent the first example of a low-temperature DAC sorbent that is purely inorganic in composition yet functions effectively from the standpoint of capture and release from humid DAC feed streams. Results presented here pave the way for exploiting a novel class of relatively inexpensive hydroxide sorbents that could help address persistent limitations associated with existing classes of DAC sorbents.

2. RESULTS AND DISCUSSION

2.1. Direct Air Capture (DAC) Performance of Nickel Hydroxides

Nickel is a common component in LDH materials containing di- and trivalent metal cations. Nickel hydroxides have two polymorphs: α-$Ni(OH)_2$, which has a hydrotalcite-like structure and contains solely divalent cations, and β-$Ni(OH)_2$, which has a similar layered structure as α-$Ni(OH)_2$ but without charge-compensating anions and water molecules in the interlayer spaces, leading to a more compact layered structure as shown in Scheme 1c.[28] β-Nickel hydroxides synthesized through coprecipitation in the absence of any template were found to carry α-$Ni(OH)_2$ impurities (Figure S1) and minimal porosity (3.3 m^2/g surface area and 0.01 cc/g pore volume, Table 1), albeit with clear characteristic diffraction peaks at 19, 33, and 39° attributable to β-$Ni(OH)_2$.[30] These textural and diffraction results are consistent with mixed nickel hydroxide phases reported previously when using chemical precipitation methods.[28] The minimal porosity of this β-nickel hydroxide sample results in an exceedingly low equilibrium CO_2 adsorption capacity under humid DAC conditions (<0.01 mmol/g, Table 1). Significant porosity was incorporated into the β-nickel hydroxide samples when applying the same coprecipitation method in the presence of an octylamine template. The templated β-$Ni(OH)_2$-T sample was found to carry a BET surface area of 240 m^2/g and a pore volume of 0.44 cc/g. The surface area obtained for this sample is within the 200−250 m^2/g range reported in prior studies employing analogous soft template-assisted (hydr)oxide syntheses.[30,31] The higher porosity of these samples resulted in a significantly greater equilibrium DAC capacity of 0.31 mmol/g under a 67% relative humidity stream (Table 1). These results suggest the potential for significantly improving DAC capacities by increasing nickel hydroxide porosity. To achieve further improvements in surface area and DAC capacity, α-$Ni(OH)_2$ samples were synthesized and subjected to an aqueous miscible organic solvent treatment (AMOST) protocol for delaminating layered double hydroxide structures. Reported by O'Hare and co-workers, this method has been shown to be effective at improving the porosity of LDH materials by redispersing wet samples into water-soluble solvents such as acetone and ethanol prior to drying.[26] Treatment with water-soluble solvents can extract water molecules out of LDH interlayers, thereby minimizing hydrogen bonding interactions and reducing the extent of particle aggregation during the drying step (Scheme 1b). Such use of solvent redispersion to improve porosity through delamination has been demonstrated previously for non-Ni-containing materials such as Mg−Al LDHs[32] and Ni−Ti LDHs, with a surface area of 492 m^2/g being achieved using an AMOST-assisted procedure for the latter,[33] attesting to the feasibility of producing highly porous metal hydroxide structures using this technique.

The powder diffraction pattern of α-$Ni(OH)_2$ reported in Figure 1a shows diffraction peaks at 2θ values of 22°, 33.6°, and 59.8° corresponding, respectively, to the (006) basal, (012), and (110) planes of α-$Ni(OH)_2$.[34] AMOST-subjected α-$Ni(OH)_2$ samples in this work carry much higher surface areas and pore volumes—820 m^2/g and 1.56 cc/g, respectively—compared to the templated and nontemplated β-nickel hydroxide samples, and also exhibit a correspondingly higher DAC capacity of 0.92 mmol/g under humid conditions (Table 1). To the best of our knowledge, this represents, to date, both the highest surface area reported in the open literature for a nickel hydroxide sample, as well as the first example of a nonalkaline earth metal hydroxide with competitive adsorption capacity and kinetics for room-temperature direct air capture. Note that unlike the sorbents reported in our study, alkaline earth metal oxide sorbents can exhibit adsorption capacities as high as 4 mmol/g at room temperature, but take extended times—sometimes up to a year—to realize this capacity,[18] rendering them impractical for low-temperature DAC specifically, and CO_2 capture at close to ambient temperatures more generally. The much smaller time scales for CO_2 diffusion and adsorption onto the PNH materials reported here, combined with the competitive equilibrium adsorption capacities presented, create an opportunity for exploiting nucleophilic oxygen/hydroxyl groups on extended surfaces for the purposes of capturing CO_2 directly from room-temperature ambient air. Next, we use aliovalent doping to rationally tune the acid−base properties of hydroxide surfaces to deliver further improvements in sorbent DAC performance.

Table 1. Textural Properties of Porous Nickel Hydroxide (PNH) Samples Tested in Our Study and Their CO_2 Adsorption Capacities in the Absence and Presence of Humidity[a]

Sample	BET surface area (m^2/g)	Pore volume (cm^3/g)	Dry DAC capacity (mmol/g)	Humid DAC capacity (mmol/g)
β-$Ni(OH)_2$	3.3	0.01	/	<0.01
β-$Ni(OH)_2$-T	240	0.44	/	0.31
α-$Ni(OH)_2$	820	1.56	0.08	0.92
α-$NiCe_{0.1}(OH)_x$	766	1.48	0.16	1.35
α -$NiFe_{0.2}(OH)_x$	476	0.47	0.18	0.53
$Ce(OH)_3$-T	116	0.16	/	0.1
α-$NiCe_{0.1}(OH)_x$-no AMOST	179	0.24	/	0.62
β-$NiCe_{0.1}(OH)_x$-T	228	0.53	/	0.48
α-$Ni(OH)_2$-SO_4^{2-}	702	1.40	/	0.99

[a]Adsorption conditions: 25 °C, 400 ppm of CO_2, 2.1 kPa H2O (67% RH)/balance N_2. Pretreatment conditions: 200 °C, Ar purge for 2 h.

https://doi.org/10.1021/jacsau.4c01083
JACS Au 2025, 5, 1649−1662

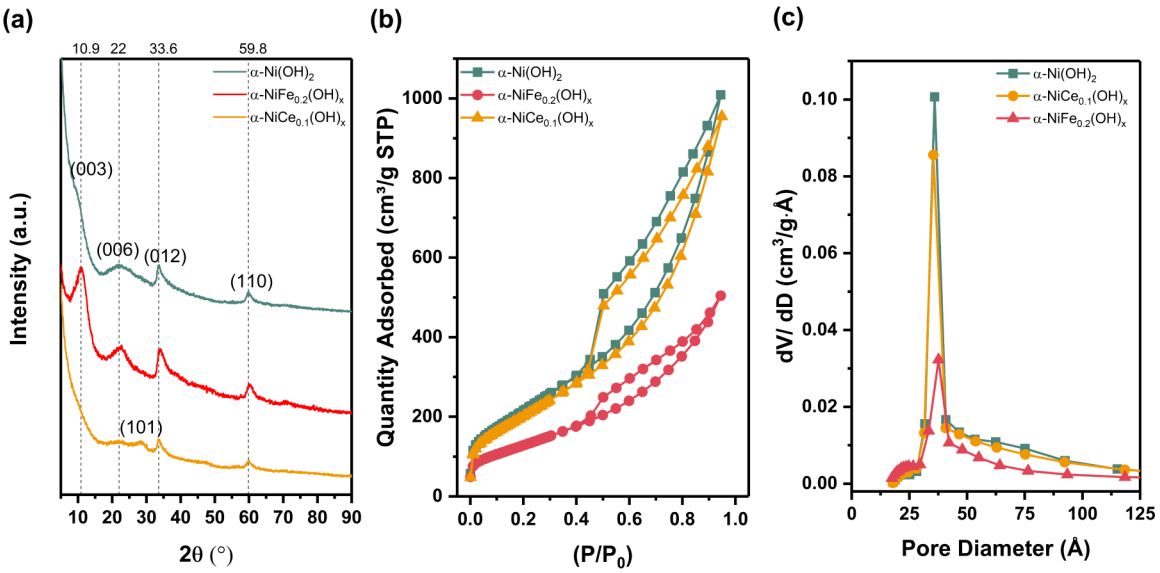

Figure 1. (a) XRD patterns of pristine samples (dashed lines represent peak positions for α-Ni(OH)$_2$), (b) N_2 adsorption−desorption isotherms, and (c) pore size distributions derived from BJH analysis of the desorption branches of the PNH sample.

2.2. DAC Performance of Doped Nickel Hydroxides

Three types of PNH samples were investigated in this work: α-nickel hydroxides (α-Ni(OH)$_2$), non-templated β-nickel hydroxides (β-Ni(OH)$_2$), and templated β-nickel hydroxides (β-Ni(OH)$_2$-T). Owing to their low surface areas and poor DAC performance, nontemplated nickel hydroxides were not further evaluated in our study. We hypothesized, consistent with density functional theory (DFT)-derived postulates put forth by the Metiu group,[35,36] that doping with metals carrying a higher valency compared to nickel will result in a net basicity on the surface that may in turn significantly increase the binding energy of CO_2. Per this postulate, when a high-valent dopant such as cerium substitutes into the NiO(H) matrix, it brings in more valence electrons compared with the nickel atom it displaces. Regardless of whether these excess electrons are delocalized onto the adjacent nickel atom or not, the excess valence electrons brought in by the high-valent dopant result in the creation of net basicity on the (hydr)oxide surface relative to the undoped surface. We hypothesized that doping of the α-nickel hydroxide sample with cerium—carrying either a + 3 or a + 4 valency—could result in a net basicity on the surface that would be reflected in the form of more nucleophilic oxygen or hydroxide moieties that would in turn bind CO_2 more strongly. Iron was also tested as an alternative dopant that could take on an oxidation state of either +2 (acting as an aliovalent dopant) or +3 (acting as a high-valent dopant). Ce/Fe-doped samples are referenced with their corresponding target mole fractions included in the nomenclature. For example, a 10 mol % Ce-doped α-nickel hydroxide sample is referred to as α-NiCe$_{0.1}$(OH)$_x$. The synthesized α-NiCe$_{0.1}$(OH)$_x$ sample exhibits similar X-ray diffraction peak positions as α-Ni(OH)$_2$, but it appears to be less crystalline than its unary counterpart (Figure 1a).

Delamination, like doping, lowers the crystallinity of the cerium-containing sample, as indicated by the presence of a more prominent diffraction peak at 11° assigned to the (003) plane of samples containing interlayer carbonates not subjected to the ethanol AMOST step (Figure S2).[37] Similar reductions in (003) peak intensity have previously been reported in other studies on nickelate layered double hydroxides after delamination steps such as AMOST or ultrasound treatment.[33,38] Delamination of the sample with ethanol results in a significant expansion in surface area (Figure S3), pointing to the effectiveness of AMOST in generating the requisite surface area for DAC applications. This ethanol treatment-derived delamination of Ni−Ce hydroxide can be demonstrated directly through its effect on particle morphology inferred from the TEM images shown in Figure 2. Whereas α-

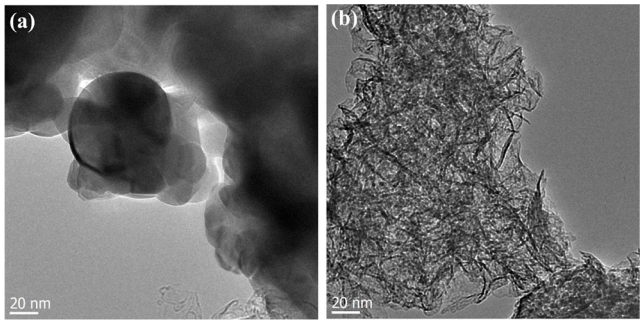

Figure 2. Bright field transmission electron microscopy (TEM) images of α-NiCe$_{0.1}$(OH)$_x$-no AMOST (a) and α-NiCe$_{0.1}$(OH)$_x$ (b).

NiCe$_{0.1}$(OH)$_x$ obtained without being subjected to AMOST treatment in ethanol shows strongly aggregated particles, the α-NiCe$_{0.1}$(OH)$_x$-6 h sample subjected to AMOST exhibits a flower-like nanosheet morphology, aligning with images for AMOST-assisted LDHs reported previously by other groups.[33,39,40] Next, we discuss the effect of Ce introduction on the structure of nickel hydroxide.

The diffraction peak attributable to the (101) plane of Ce(OH)$_3$ that appears at 28° upon introduction of cerium (Figure 1a)[41] suggests that not all of the cerium substitutes isomorphously into the NiO matrix. Unlike the demonstrably heterogeneous α-NiCe$_{0.1}$(OH)$_x$ material in which a fraction of the cerium is present as a separate Ce(OH)$_x$ phase, the α-NiFe$_{0.2}$(OH)$_x$ material is significantly more crystalline than the single-component α-Ni(OH)$_2$ sample (Figure 1a). The absence of additional diffraction peaks upon the introduction

https://doi.org/10.1021/jacsau.4c01083
JACS Au 2025, 5, 1649−1662

of Fe suggests minimal formation of crystalline $Fe(OH)_x$ phases, and the sharper diffraction peaks -- including the appearance of a clear (003) peak at 11° -- suggest the formation of a much more crystalline α-Ni hydroxide phase upon doping with Fe. Besides, the (003) and (006) basal plane peaks in α-$NiFe_{0.2}(OH)_x$ that appear shifted to higher 2θ values compared to α-$Ni(OH)_2$ suggest a shorter basal spacing, consistent with lesser delamination and a greater extent of stacking for the Fe-containing sample. The (012) and (110) diffraction peaks are also shifted to slightly higher 2θ values (Figures S4 and S5), likely originating from lattice substitution of Fe^{3+} ions carrying a smaller ionic radius (0.0645 nm) compared to Ni^{2+} ones (0.069 nm). Note that the similar positions of Fe and Ni in the periodic table imply that the minimal shift in diffraction peak position is expected even if the entirety of the Fe was isomorphously substituted into the Ni−OH lattice. In fact, the similar ionic radii of Fe and Ni may constitute part of the reason for the more effective substitution of Fe and the concomitant absence of diffraction peaks corresponding to crystalline $Fe(OH)_3$. We posit that unlike $Ce^{3+/4+}$ ions that have a negligible effect on the pore properties of the synthesized hydroxide, strong particle aggregation is retained in the α-$NiFe_{0.2}(OH)_x$ sample, presumably due to Fe^{3+}-induced stabilization of layer stacking that is resistant to delamination upon redispersion in ethanol.

Consistent with the X-ray diffraction results, the α-$Ni(OH)_2$ and α-$NiCe_{0.1}(OH)_x$ samples exhibit similar pore characteristics including surface area and pore diameter, unlike the much more crystalline α-$NiFe_{0.2}(OH)_x$ sample that exhibits a lower surface area (476 m^2/g), albeit with a similar pore diameter (Table 1 and Figure 1b,c). The lower surface area of the Fe-containing sample reinforces our assertion that it is in fact delamination of the α-$Ni(OH)_2$ structure that enables the creation of very high surface areas for the α-$Ni(OH)_2$ and α-$NiCe_{0.1}(OH)_x$ samples (820 and 766 m^2/g, respectively, Table 1). The more ordered and stable layered structure formed upon the introduction of Fe into α-$Ni(OH)_2$ in fact *disfavors* the creation of the requisite degree of porosity for DAC applications. Textural properties of samples reported here, including a type-IV isotherm with an H3-type hysteresis loop, mirror prior reports on LDH samples subjected to AMOST protocols,[26,33] and point to particle stacking as the predominant source of sample porosity. The mesoporosity corresponding to this hysteresis loop could also potentially originate from the presence of non-rigid aggregates of plate-like particles present in a layered material.[42] FTIR spectra of the α-$Ni(OH)_2$ and α-$NiCe_{0.1}(OH)_x$ samples contain infrared bands at 2974 cm^{-1} likely corresponding to C−H stretching vibrations originating from residual interlayer ethanol molecules recalcitrant to thermal treatment at 200 °C; the spectra also point to the presence of intercalated carbonate anions that exhibit symmetric stretching bands at 1378 cm^{-1} (Figure S6).[33,37,43]

Figure 3 shows a compilation of DAC capacities in the presence of water vapor for the various unary and binary α- and β-nickel hydroxides as a function of their corresponding BET surface areas. DAC capacities for all samples devoid of Ce were found to be linearly correlated with surface area irrespective of crystal structure, Ni/Fe content, and AMOST treatment, suggesting that variations in DAC capacity in these samples can be attributed entirely to changes in surface area and the corresponding concomitant alterations in adsorption site density but not to the tuning of acid−base properties that

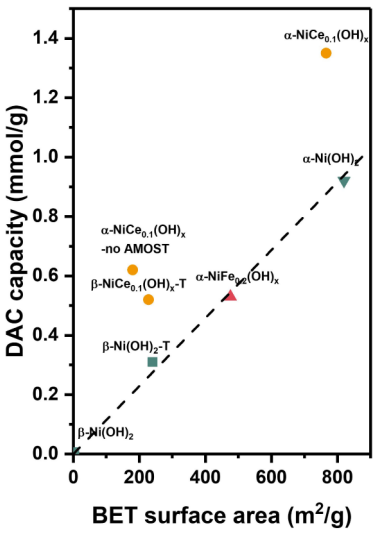

Figure 3. DAC capacities of various porous nickel hydroxides plotted as a function of BET surface area. Adsorption measurements were carried out at 25 °C under 400 ppm of CO_2, 2.1 kPa of H_2O (67% RH), and balance N_2. Dashed line represents a linear regression for the adsorption capacities of the Ce-free sorbents.

result from changes in coordination environments of active oxygens or hydroxyls. Doping with Fe fails to result in an enhancement in DAC performance on a per unit surface area basis despite the highly crystalline nature of the sample and the absence of diffraction peaks associated with crystalline $Fe(OH)_x$. In contrast, every Ce-containing nickel hydroxide sample tested exhibits a disproportionately higher adsorption capacity compared with the corresponding non-Ce analogues at equivalent surface areas (Figure 3). Specifically, the templated Ce−Ni β-hydroxide sample was found to exhibit a significantly larger adsorption capacity compared to the Ni β-hydroxide sample (0.48 versus 0.31 mmol CO_2/g) despite carrying a slightly smaller BET surface area (228 versus 240 m^2/g). Moreover, the Ce−Ni α-hydroxide sample subjected to AMOST manifested the highest DAC capacity of all materials tested (1.35 mmol CO_2/g), and also, to the best of our knowledge, the highest DAC capacity measured at reasonable time scales reported to date in the literature under ambient conditions for materials that are either oxidic or hydroxidic in composition. Improvements in DAC capacity are significant; for example, a 47% increase in the adsorption capacity was noted upon doping α-$Ni(OH)_2$ with cerium. These improvements in DAC performance are unlikely to be a consequence of $Ce(OH)_x$ domains formed upon addition of Ce to α-$Ni(OH)_2$ because areal CO_2 adsorption capacities for $Ce(OH)_3$-T are much lower than those for α-$NiCe_{0.1}(OH)_x$ (0.0009 versus 0.0018 mmol of CO_2/m^2). They instead appear to result from a synergistic effect of isomorphous doping of Ce that perturbs the surface chemistry of the adsorption site. Differences in water adsorption or hydroxyl formation are also unlikely to be contributing factors to these improvements, as reflected in the near-identical water adsorption isotherm data for the α-$Ni(OH)_2$ and α-$NiCe_{0.1}(OH)_x$ samples (Figure S7). We therefore ascribe the larger DAC capacities for Ce-containing samples to an effect of doping that is consistent with the aforementioned hypothesis that substitution with high-valent dopants increases the basicity of the nickel (hydr)oxide surface. Our XPS results provide further

https://doi.org/10.1021/jacsau.4c01083
JACS Au 2025, 5, 1649−1662

Scheme 2. Possible Adsorption Mechanisms Mediating CO_2 Binding onto PNH Materials Including (a) CO_2 Binding in the Form of Interstitial Bicarbonates within Anion Interlayers, (b) CO_2 Adsorption onto Surface Hydroxyls, and (c) CO_2 Binding Enabled by the Molecular Adsorption of Water

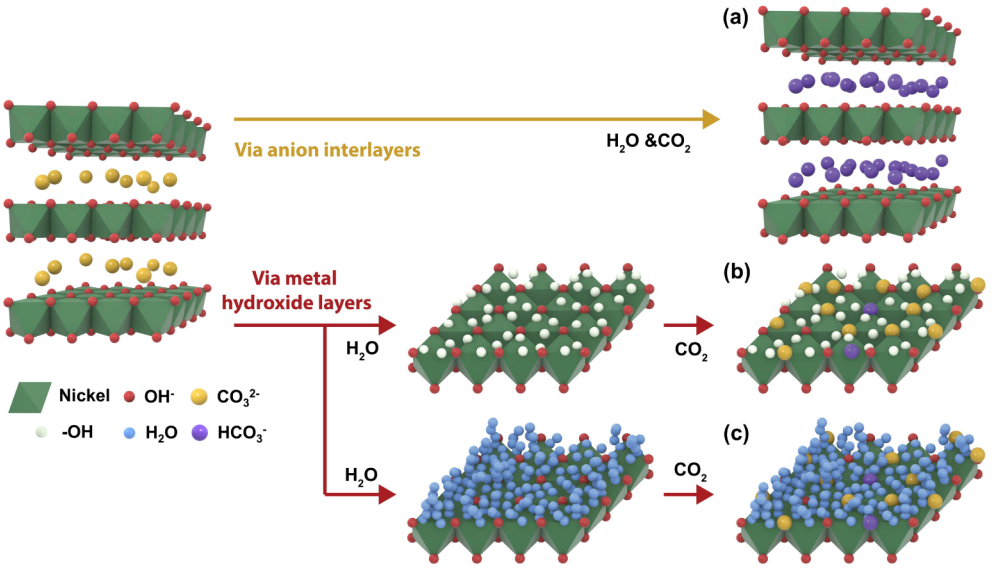

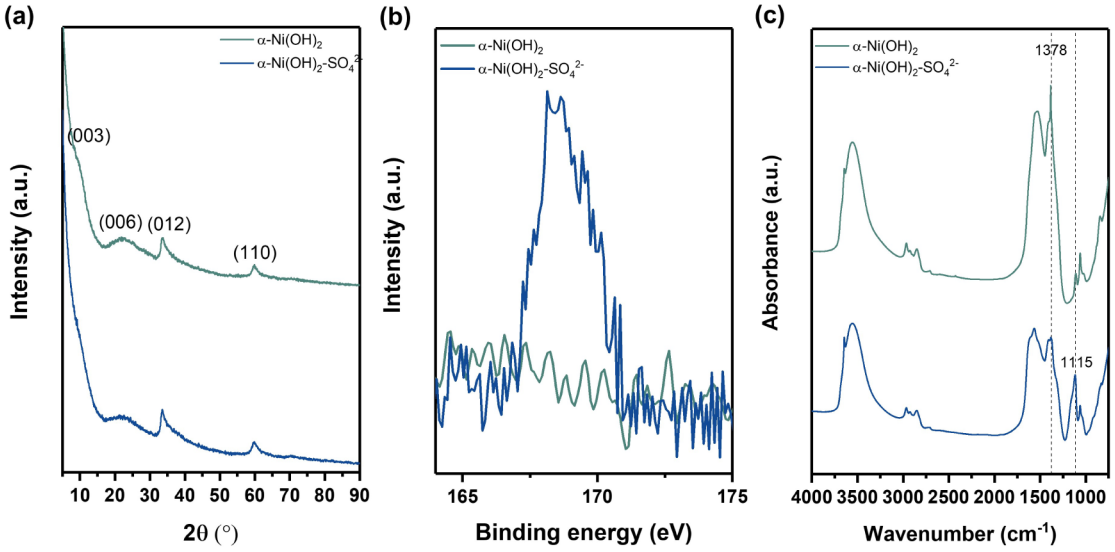

Figure 4. (a) Powder X-ray diffraction patterns, (b) S 2p XPS spectra, and (c) FTIR spectra of α-$Ni(OH)_2$ and α-$Ni(OH)_2$-SO_4^{2-} samples obtained at 30 °C under an Ar purge after a 2 h, 200 °C thermal pretreatment under Ar.

corroborating evidence of the alteration of surface hydroxide binding characteristics through doping. The Ni 2p peak in the XPS data shown in Figure S8 shifts to higher binding energies from 855.3 eV for α-$Ni(OH)_2$ to 855.65 eV for α-$NiCe_{0.1}(OH)_x$, indicating partial electron transfer out of the Ni^{2+} ion upon Ce^{3+} introduction; such electron transfer is consistent with more electron rich (i.e. more basic) oxygen/hydroxyl moieties. These more basic moieties would in turn explain the higher DAC capacities under both dry and humid conditions upon the introduction of cerium into the α-$Ni(OH)_x$ matrix. Similar changes in Ni 2p binding energy have been suggested by Liu et al. to result in lower overpotentials for oxygen evolution reaction catalysis over $Ce(OH)_3$-containing and Ce-doped NiFe-LDH materials.[44] We note that other XPS regions may be less informative as the binding energies of the O electron may be affected due not only to Ce dopant effects but also the formation of distinct $Ce(OH)_3$ phases the contributions of which are challenging to deconvolute; these phases would result in binding energy shifts even in the absence of a perturbation of Ni−OH lattice oxygens.

The basis for the limited effect of Fe doping on adsorption capacities noted in Figure 3 remains ambiguous, but could be attributed to the fact that Fe, unlike Ce, can carry either a + 2 or a + 3 oxidation state. Note that doping with either of the elements considered—Fe or Ce—increases DAC capacities on a per unit area basis under dry conditions, but only doping with Ce results in an improvement in performance under wet conditions (Table 1). Crucially, all nickel hydroxide samples tested in our work, regardless of chemical composition or crystal structure, benefit from the presence of humidity in the

https://doi.org/10.1021/jacsau.4c01083
JACS Au 2025, 5, 1649−1662

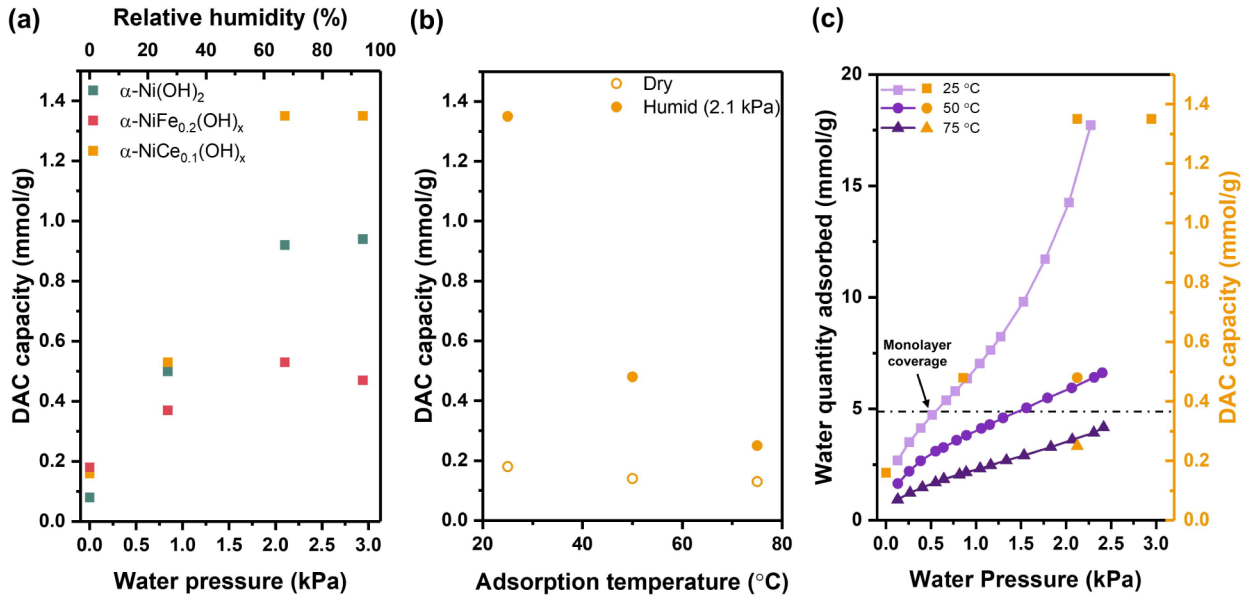

Figure 5. (a) DAC adsorption capacity as a function of water pressure for the three α-Ni(OH)$_2$ materials tested, adsorption under 400 ppm of CO$_2$ at 25 °C, (b) effect of adsorption temperature on α-NiCe$_{0.1}$(OH)$_x$ DAC capacities under dry and humid (2.1 kPa water) conditions, and (c) water adsorption isotherms for α-NiCe$_{0.1}$(OH)$_x$ at 25, 50, and 75 °C, and DAC capacities at the corresponding adsorption temperatures and water pressures. The horizontal dashed line represents the estimated water monolayer coverage for α-NiCe$_{0.1}$(OH)$_x$ at 3.6 molecules/nm^2.

feed stream. We next discuss the effect of Ni−OH surface hydration on CO$_2$ binding characteristics.

2.3. Effect of Water on CO$_2$ Binding

Consistent with prior reports,[45] we find that metal hydroxides are not optimal candidate sorbents for CO$_2$ capture under dry conditions owing to the minimal binding that they exhibit in the absence of humidity. This conclusion changes, however, when evaluating this class of sorbents in the presence of water vapor, prompting questions as to the basis for the favorable role of water on CO$_2$ binding. Three potential types of sites were considered in our analysis of CO$_2$ adsorption data (Scheme 2)—interlayer carbonates, surface hydroxyls, and adsorbate species stabilized by surface water. Interlayer carbonates can react chemically with CO$_2$ in the presence of water to form bicarbonate species, akin to low-pressure CO$_2$ adsorption mechanisms proposed previously over sodium/potassium carbonate-impregnated sorbents that form bicarbonate species in the presence of water vapor.[46−48] To test the contribution of interlayer carbonates to CO$_2$ adsorption, an SO_4^{2-}-exchanged α-Ni(OH)$_2$ sample was synthesized by redispersing the α-Ni(OH)$_2$ wet cake obtained after washing with DI water into an aqueous sodium sulfate solution for 48 h at room temperature. The sulfate-exchanged sample was found to exhibit a powder X-ray diffraction pattern and porosity similar to those of the native α-Ni(OH)$_2$ sample (Figures 4a, S9 and Table 1). Sulfate ion exchange can be evidenced by the appearance of an S 2p peak at 168.35 eV in the XPS spectrum of the α-Ni(OH)$_2$-SO_4^{2-} sample that is absent in the case of the α-Ni(OH)$_2$ sample (Figure 4b), as well as the appearance of a new infrared band at 1115 cm^{-1} attributable to the asymmetric stretching mode of the sulfate anion and the concomitant loss of carbonate symmetric stretching bands at 1378 cm^{-1}.[49] Roughly half the area of the carbonate band at 1378 cm^{-1} was lost during ion exchange, suggesting significant but partial exchange of carbonate species with sulfate anions despite the limited propensity toward anion exchange suggested by the strong binding of carbonates onto metal hydroxide layers evidenced previously using experiment and theory.[37,50] The involvement of interlayer carbonates in CO$_2$ adsorption would require that the adsorption capacities drop significantly upon sulfate ion exchange. Similar DAC capacities measured pre- versus post-ion exchange (0.92 versus 0.99 mmol CO$_2$/g), however, appear to eliminate the potential involvement of interlayer carbonates in CO$_2$ adsorption (pathway a, Scheme 2) and suggest that CO$_2$ may instead bind to either surface hydroxyls or other sites that are "activated" in the presence of water (pathways b and c, Scheme 2). Note that the strong correlation between DAC capacities and BET surface areas captured in Figure 3 and the positive influence of delamination of the layered structure on CO$_2$ capture performance both provide further corroboration of the participation of surface, not interlayer sites, in CO$_2$ adsorption.

The presence of water has a significant favorable effect on the CO$_2$ adsorption capacities of all of the nickel hydroxide materials tested. CO$_2$ adsorption capacities increased with water partial pressures up to 2.1 kPa water before plateauing out or decreasing slightly at higher pressures (Figure 5a). The presence of water could either a) merely increase the density of adsorption sites present or b) alter not only the density but also the CO$_2$ binding characteristics of these sites. The much greater sensitivities of adsorption capacities to adsorption temperature under humid conditions compared to under dry conditions (Figure 5b) suggest a significant increase in binding energy in the presence of water versus in its absence. As an example, adsorption capacities of α-NiCe$_{0.1}$(OH)$_x$ decrease by 81% when increasing the adsorption temperature from 25 to 75 °C under 2.1 kPa water vapor but only by 28% for the same change in temperature under dry conditions. The larger changes in adsorption capacity under humid conditions could also be a consequence of the lower water loadings encountered at higher temperatures under wet conditions, unlike dry conditions where the surface carries minimal amounts of water regardless of adsorption temperature. The presence of water vapor affects not only the adsorption capacity values but also

https://doi.org/10.1021/jacsau.4c01083
JACS Au 2025, 5, 1649−1662

our interpretation of the effect of doping on CO_2 binding. Under dry conditions, α-$NiFe_{0.2}(OH)_x$ and α-$NiCe_{0.1}(OH)_x$ capture more CO_2 on a per unit area basis compared to α-$Ni(OH)_2$ (Table 1), unlike under humid conditions where only the Ce, not the Fe-containing sorbent, exhibits higher areal DAC capacities (Figure 3). Adsorption energies under dry conditions measured using microcalorimetry are shown in Figure 6, and they demonstrate that the higher DAC capacities

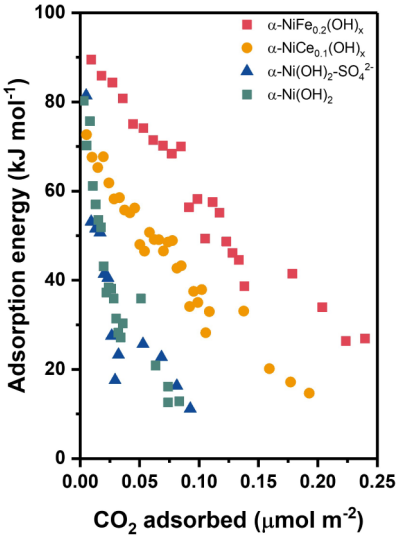

Figure 6. CO_2 adsorption energies of PNH materials measured using microcalorimetry at incrementally increased CO_2 pressure at 30 °C. Samples were thermally pretreated for 2 h under vacuum at 200 °C prior to CO_2 adsorption.

on the Fe- and Ce-doped materials result from stronger binding compared to the unary α-Ni hydroxide sample. Adsorption energies over a wide range of surface coverages follow the order α-$NiFe_{0.2}(OH)_x$ > α-$NiCe_{0.1}(OH)_x$ > α-$Ni(OH)_2$/α-$Ni(OH)_2$-SO_4^{2-}—identical to the order of areal DAC capacities under dry conditions. These calorimetry data provide strong evidence of the enhanced CO_2 adsorption strength upon doping with Fe or Ce, potentially resulting from the expected enhancement in basicity of hydroxide moieties in the presence of high-valent dopants. These contrasting effects of doping in the presence and absence of water vapor demonstrate a unique role of water in facilitating the binding of CO_2.

These significant changes in binding energy could originate either from the creation of hydroxyls generated through the dissociative adsorption of water (pathway b, Scheme 2) or from the direct involvement of molecularly adsorbed water in CO_2 binding (pathway c, Scheme 2). Analysis of water adsorption isotherms measured over α-$NiCe_{0.1}(OH)_x$ provides insights that help further differentiate between these two adsorption pathways. A type II water isotherm indicative of monolayer−multilayer adsorption was measured at 25 °C, with an inflection in the range of 0.45−0.55 kPa corresponding to a transition from monolayer to multilayer adsorption (Figure 5c). Surface hydroxylation, unlike water adsorption, is necessarily constrained to the nickel hydroxide surface and hence should cease to provide improvements in DAC adsorption performance past the water vapor pressure where hydroxyl/water monolayers are formed. In sharp contrast with this expectation, DAC capacities continue to increase significantly even above pressures that result in monolayer coverages of water (Figure 5c). Not only do multilayer water adsorption capacities continue to favorably impact CO_2 adsorption but also in fact seem to provide a marker for CO_2 adsorption capacities. DAC capacities shown in Figure 5c track quantitatively with water adsorption at multiple pressures at a tempertaure of 25 °C, and at multiple adsorption temperatures at a water pressure of 2.1 kPa. The strong correlation between the quantities of bound water and CO_2 adsorbed over a wide range of mono- and multilayer coverages suggests a role of molecular water clusters in enhancing CO_2 binding onto nickel hydroxide surfaces (pathway c, Scheme 2). Note that the involvement of molecular water in CO_2 binding

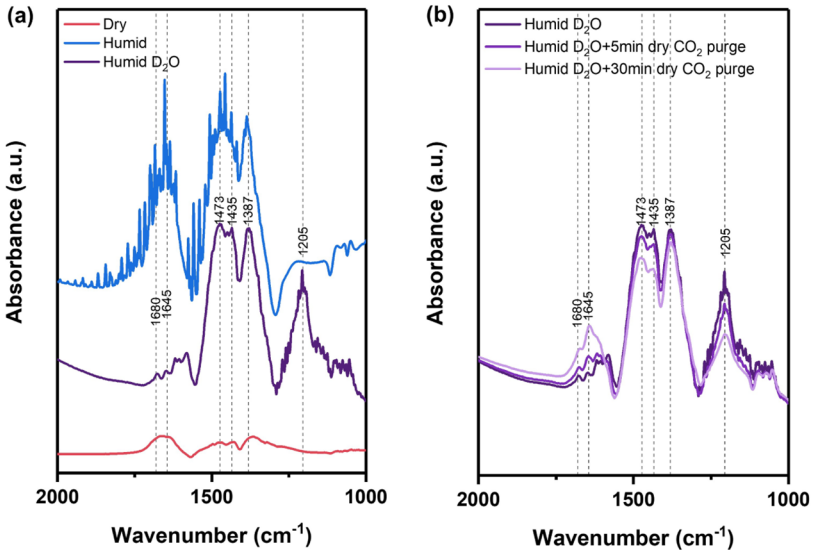

Figure 7. FTIR spectra of α-$Ni(OH)_2$ measured under 400 ppm CO_2 without water vapor (dry), 400 ppm CO_2 and 2.1 kPa H_2O (humid), and 400 ppm CO_2 and 2.1 kPa D_2O (humid D_2O). (b) Evolution in FTIR spectral data over α-$Ni(OH)_2$ upon switching from a stream containing 400 ppm CO_2 and 2.1 kPa D_2O (humid D_2O) to one containing only 400 ppm CO_2; spectra are reported either 5 or 30 min after switching to a dry stream. Reported spectra are background subtracted from those measured under Ar before exposure to CO_2.

https://doi.org/10.1021/jacsau.4c01083
JACS Au 2025, 5, 1649−1662

does not in and of itself disprove participation of surface hydroxyls; rather, CO_2 binding could still occur over surface hydroxyls in a manner that is facilitated by either molecular water or hydrogen-bonded water clusters. A possible explanation for the facilitative role of water is the formation of a particular type of precursor species in the condensed phase that then coordinates to the hydroxide surface, akin to the mechanism for CO_2 binding onto hydroxide-bearing polyamine-Cu(II) hybrid sorbents proposed recently by the Sengupta group.[51] The favorable effect of water vapor upto relative humidity values of 60% on CO_2 adsorption was interpreted in their work to result from acid−base interactions not between surface sites and CO_2 but instead between surface hydroxides and carbonic acid, the latter of which was preformed through CO_2 dissolution into the condensed water phase. Adsorbed water also appears to enable the binding of CO_2 onto nickel hydroxide samples tested in our study, although its precise role—which could potentially include solvation of bound species or the formation of unidentified precursors to these bound species—remains ambiguous at this point, and constitutes the focus of current and future investigation. We note that the facilitative role of water in CO_2 adsorption sensed here contrasts with hydroxide-bearing MOFs that can exhibit only limited tolerance to water vapor, as well as an outsized propensity toward degradation in the presence of oxygen.[21,27] Nickel hydroxides reported here, in contrast, are highly water-tolerant, as demonstrated through the data in Figure 5, and highly oxidatively stable, as discussed in Section 2.5. We probed next, using infrared spectroscopy, the speciation of adsorbed CO_2 under dry and humid conditions.

2.4. Adsorbate Speciation under Dry and Humid Conditions

In situ FTIR measurements over α-Ni$(OH)_2$ under 400 ppm of CO_2 reveal a series of infrared bands between 1000 and 1700 cm^{-1} that correspond to carbonate and bicarbonate species (Figure 7a). Symmetric and asymmetric stretching modes for (bi)carbonate species in the 1000−1700 cm^{-1} wavenumber range have been reported widely in the literature, and band positions are shown to vary with metal (hydr)oxide identity and surface coordination environment.[21,23,31,52] We assign bands at 1645 and 1680 cm^{-1} detected in the presence of 400 ppm of CO_2 under dry conditions to asymmetric stretching modes for HCO_3^- species that have previously been reported to appear in the 1580−1680 cm^{-1} range during CO_2 adsorption over a variety of hydroxyl-bearing materials including MOFs, reducible bulk metal oxides, and hydrotalcites.[18,21,22,31,52] The three bands at lower wavenumbers—1387, 1435, and 1473 cm^{-1}—can be assigned to O−C−O stretching modes for CO_3^{2-} species.[18,31,53] The inclusion of 2.1 kPa water vapor in the 400 ppm CO_2 stream results in a significant increase in each of the aforementioned carbonate and bicarbonate bands (Figure 7a), consistent with the much higher DAC capacities under humid conditions compared to those under dry conditions (Table 1 and Figure 5a). These infrared bands, however, are rendered challenging to discern due to the presence of features corresponding to H−O−H bending vibrations in the 1600−1700 cm^{-1} range when cofeeding H_2O. These bands become more apparent when using D_2O cofeeds rather than H_2O cofeeds because D−O−D bending modes appear as a distinguishable band near 1205 cm^{-1} rather than the 1600−1700 cm^{-1} range that now appears well-defined and distinct from H−O−H bending vibrations previously obfuscating key infrared features (Figure 7a). Positions of bands associated with carbonates that are devoid of hydrogen/deuterium are unaffected by the introduction of D_2O, unlike bands assigned to hydrogen/deuterium-containing bicarbonates that redishift from 1645 and 1680 cm^{-1} to 1585 and 1618 cm^{-1}, respectively, providing further corroboration our infrared virbational assignments. These effects of H−D substitution are also consistent with previously reported IR band red-shifts for $KDCO_3$ and $KHCO_3$ powders calculated using DFT and measured experimentally.[54] The coexistence of both protonated and deuterated bicarbonates in the presence of D_2O is not entirely unexpected since surface hydroxyls need not be completely exchanged with deuterium; infrared band intensities at 1645 and 1680 cm^{-1} are minor compared to those at 1585 and 1618 cm^{-1}, suggesting that the surface is mostly (but not completely) deuterated. Intriguingly, the three bands at 1387, 1435, and 1473 cm^{-1} assigned to carbonate species were amplified disproportionately upon introduction of D_2O compared to the bands at 1645 and 1680 cm^{-1} ascribed to bicarbonate species, with the latter showing little growth in intensity upon switching to humid conditions. The introduction of D_2O therefore appears to favor the formation of carbonates rather than bicarbonates despite the fact that the formation of bicarbonates (presumably) involves hydrolysis of carbonates by means of the following reaction:[55]

$$CO_3^{2-} + H_2O \rightarrow HCO_3^- + OH^-$$

If the thermodynamics of the hydrolysis reaction were the only factor determining adsorbate speciation, one would expect increasing water concentrations to lead to higher bicarbonate-to-carbonate molar ratios. The predominance of carbonates under wet conditions, and bicarbonates under dry conditions, appears to instead suggest factors other than the carbonate−bicarbonate reaction equilibrium determining adsorbate speciation.

The preferential formation of carbonate species in the presence of water (depicted in Scheme 3) has been reported widely in the open literature. Gankanda et al.,[56] for instance, evidenced the progressive solvation of carbonates with increasing relative humidities over copper and zinc oxide nanoparticles by identifying unique infrared bands at 1385 and 1490 cm^{-1} that increased in intensity relative to unsolvated

Scheme 3. Depiction of the Proposed Effect of Hydration on the Free Energies of (Bi)Carbonates Formed through CO_2 Binding onto Metal Hydroxide Surfaces

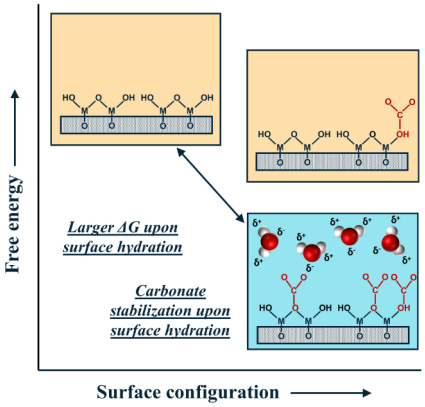

https://doi.org/10.1021/jacsau.4c01083
JACS Au 2025, 5, 1649−1662

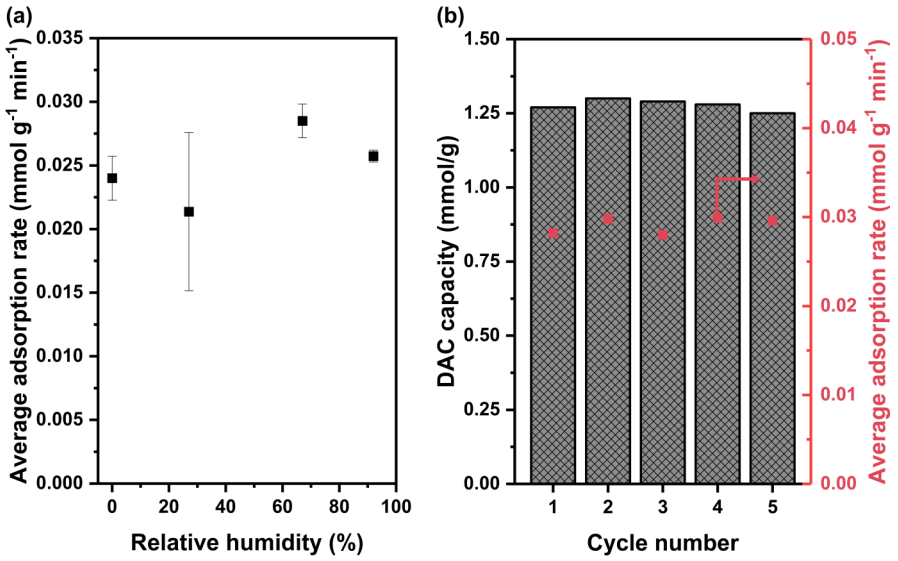

Figure 8. (a) Average adsorption rates for α-$NiCe_{0.1}(OH)_x$ as a function of the relative humidity of the feed stream. Rates were calculated from breakthrough curves measured at 25 °C under 400 ppm CO_2. (b) Cyclic DAC performance of α-$NiCe_{0.1}(OH)_x$ over 5 cycles. Adsorption conditions: 25 °C, 400 ppm CO_2, balance N_2. Regeneration conditions: 100 °C for 2 h under 2.1 kPa H_2O, 20 kPa O_2, balance Ar.

carbonates. The preferential formation of carbonates has also been proposed in the context of moisture swing adsorption processes over ion exchange resins; these sorption systems entail CO_2 adsorption under dry conditions and desorption under humid conditions.[57−59] The Chen group used molecular dynamics simulations to study the effect of up to 10 molecules of water per molecule of adsorbate on free energy changes for carbonate−bicarbonate interconversion over ion exchange resins containing quaternary ammonium salts. They reported that the free energy of carbonates relative to bicarbonates decreased monotonically with increasing surface water:carbon ratios.[57] They also deconvoluted the effect of solvation from that of the carbonate−bicarbonate reaction equilibrium and found that while both these surface species were solvatively stabilized to a similar extent in the absence of water, solvation preferentially stabilizes carbonate over bicarbonate species with increasing water:carbon ratios.[58] These simulations not only point to solvation as being a predominant factor affecting CO_2 speciation in confined environments but also suggest that the stability of carbonates is affected more sensitively upon initial addition of water molecules than surplus hydration provided at higher water:carbon ratios. For instance, per these calculations, preferential solvation ceases to affect carbonate stability above a value of 20 molecules of water per carbonate ion.[58] Adsorbate valency also plays a determinative role in solvative stabilization, as shown by Shi et al. in their study on the hydrolysis of a variety of mono-, di-, and trivalent ions. Their conclusion that the preferential solvation of carbonate species extends to other divalent (and even trivalent ions), but not monovalent ions, suggests that the difference in valency between divalent carbonate and monovalent bicarbonate anions could constitute a potential basis for the stabilization proposed in our work.[55] Analogies between CO_2 capture by porous nickel hydroxides reported here and moisture swing adsorption proposed by the Lackner group also extend to wet-to-dry transients.[60] Purging a sample under 400 ppm CO_2 and 2.1 kPa D_2O with a stream containing 400 ppm CO_2 in the absence of D_2O resulted in a monotonic decrease in carbonate coverage and a concurrent monotonic increase in bicarbonate coverage (Figure 7b), suggesting that the stabilization of carbonates at high water loadings is indeed reversible, akin to moisture swing adsorbents that respond reversibly to changes in humidity under isothermal conditions.[58,60] Not only does the adsorbate speciation mirror that observed in moisture swing adsorption, but so do adsorption capacities, as evidenced by the fact that a small but measurable amount of CO_2 (0.04 mmol CO_2/g) is adsorbed upon switching from humid to dry conditions (Figure S10). These results capture not only the analogous nature of carbonate−bicarbonate interconversion chemistry sensed in our experiments versus those reported under wet conditions on other classes of sorbents but also point to some intriguing differences between the adsorption chemistry prevalent on nickel hydroxide surfaces under wet versus dry conditions. Crucially, we note that the solvative stabilization of carbonates under humid conditions has thus far, been exploited solely for moisture swing applications, not temperature swing adsorption applications that are more commonly evaluated for direct air capture; to the best of our knowledge, the data on porous nickel hydroxides reported here represents the first instance of its application in realizing viable temperature swing adsorption capacities for DAC applications. Adsorption in the form of carbonates enables not only the reversible adsorption of CO_2 at low temperatures but also rapid adsorption kinetics and robust cyclic stability under aggressive oxidative conditions, as discussed next.

2.5. Adsorption Kinetics and Cyclic Oxidative Stability

In addition to equilibrium adsorption capacities, adsorption kinetics that determine DAC working capacities are another key performance metric, with rapid kinetics enabling shorter cycle times and minimizing DAC costs.[61] In fact, one of the primary limitations of inorganic metal oxide or hydroxide sorbents such as MgO and CaO is the slow room-temperature adsorption kinetics that adversely affect the performance of these materials. The PNH materials reported here, on the other hand, exhibit uptake kinetics that compare favorably with those of other classes of organic−inorganic hybrid sorbents such as supported amines that represent the state-of-the-art for temperature swing DAC applications. The average adsorption

https://doi.org/10.1021/jacsau.4c01083
JACS Au 2025, 5, 1649−1662

rate for α-$NiCe_{0.1}(OH)_x$ calculated based on the adsorption half-time compares favorably with values reported previously for a variety of supported amine sorbents listed in Table S1.[62−65] Note that the different techniques and flow conditions used in these studies render quantitative comparison challenging to conduct and limited in rigor; the data nevertheless still strongly support the viability of practical operation over nickel hydroxides with sufficiently fast adsorption cycles. As shown in Figure 8a, adsorption uptake rates are affected only slightly by the relative humidity of the CO_2 feed stream, meaning that wet DAC feeds still benefit from larger equilibrium capacities without an adverse effect on uptake kinetics that could potentially result as a consequence of adsorbed water multilayer formation. Water therefore facilitates binding without inducing severe gas−liquid diffusion limitations. An exception to this trend appears to be the data point at the lowest relative humidity tested (27%). Comparison of the breakthrough curves at different relative humidities (Figure S11) indicates that the outlet CO_2 concentration at the adsorption half-time is significantly higher for the run at 27% relative humidity. A likely cause of these poorer kinetics is the more gradual progression of the water adsorption front at lower water vapor pressures, thereby potentially leading to a larger fraction of the CO_2 being adsorbed at later times in the breakthrough experiment when high water loadings are accumulated on the sorbent surface. A more detailed analysis of dynamic breakthrough phenomena is needed in order to fully explain these trends in adsorption kinetics. Crucially though, adsorption time scales consistently remain of a similar order of magnitude as those exhibited by supported amines, and orders of magnitude smaller than those for many of the previously reported oxide sorbents that only operate efficaciously at higher, but not ambient temperatures.

Cyclic stability of DAC sorbents under oxidative conditions is another key factor determining sorbent lifetime and total cost. Sorbents such as supported amine materials containing organic components are inherently susceptible to oxidative and hydrothermal degradation, for example at 75 °C after 12 h of aging under air at 105 °C.[66] Gebald et al. reported a 30% loss in DAC capacity for amine-functionalized nanofibrillated cellulose sorbents after treatment for 15 h under a humid 20% O_2 in N_2 stream at 90 °C.[67] Carneiro et al. recently suggested that the presence of water vapor can accelerate oxidative degradation of alumina-supported PEI by a factor of 2 compared to that under dry conditions.[68] Other potentially irreversible side reactions such as urea formation and leaching of organics further complicate the use of supported amine sorbents despite their competitive adsorption capacities and kinetics. PNHs are expected to serve as a highly robust platform for cyclic experiments in the presence of oxygen given the fact that surface oxygen/hydroxyl groups that capture CO_2 are already rich in oxygen and hence less susceptible to oxidation. α-$NiCe_{0.1}(OH)_x$ exhibits excellent cyclability when regenerated at 100 °C under a stream containing 2.1 kPa steam and 20 kPa O_2 (Figures 8b and S12). Imperceptible extents of degradation were observed over the course of 5 temperature swing adsorption−desorption cycles, with the adsorption capacity remaining stable at 1.25 mmol CO_2/g. Adsorption kinetics also remained robust to cycling, with the adsorption rate remaining close to a value of 0.028 mmol g^{-1} min^{-1}. The consistent performance noted over 5 cycles despite the rather aggressive hydrothermal and oxidative conditions used during regeneration points to the potential for the α-$NiCe_{0.1}(OH)_x$ samples tested here to be subjected to extensive cycling under real-world DAC conditions.

Table S2 provides further comparison of the DAC performance of our sample with other sorbents reported in the prior literature.[5,8,9,69−72] The working capacity of α-$NiCe_{0.1}(OH)_x$ is highly competitive with that of zeolites, MOFs, and supported amine sorbents that have undergone testing for water tolerance and cyclic stability. Complete regeneration is achieved at a mild regeneration temperature of 100 °C in the presence of steam and oxygen, rendering it competitive versus supported amine materials that are hampered by oxidative degradation at elevated temperatures. Zeolites oftentimes require temperatures greater than 250 °C to achieve complete regeneration, with a few exceptions like Zn-CHA that have been shown to exhibit 90% regeneration at 100 °C.[5,8,73] The water tolerance of PNH samples used herein bodes well from the standpoint of commercial application, given that most physisorbents reported to date show either significant competitive adsorption of water or limited hydrothermal stability (Table S2). Even SIFSIX-18-Ni-β—one of the most water-tolerant MOFs reported—nevertheless shows a 57% drop in capacity under a relative humidity of 74%.[9] The stable cyclic performance of PNH samples appears unprecedented in light of these prior studies, and could extend broadly to other formulations within this novel class of inorganic sorbents—sorbents that thus far appear to compare favorably on every apparent performance metric of relevance to DAC applications.

3. CONCLUSIONS

Aqueous miscible organic solvent treatment of nickelate layered double hydroxide structures yields high-surface-area porous nickel hydroxides (PNHs) that capture little CO_2 under dry conditions, but exhibit competitive DAC capacities when exposed to humid air streams. Both of the high-valent dopants tested—Fe and Ce—result in an increase in areal adsorption capacity under dry conditions, unlike under wet conditions, where only doping with Ce results in DAC capacity enhancement. Unlike many other classes of DAC sorbents, the presence of humidity has a significant favorable effect on equilibrium DAC capacities and a minimal impact on adsorption kinetics for all PNH sorbents tested, with adsorption kinetics shown to compare favorably with supported amine sorbents heavily evaluated in the open literature. The favorable effect of water on DAC performance manifests over a wide range of mono- and multilayer water coverages, and appears to originate from the preferential stabilization of carbonates in the presence of adsorbed water. Infrared spectra confirm the transformation of bicarbonate species formed on PNH surfaces under dry conditions to carbonate species under humid conditions, akin to changes in adsorbate speciation in moisture swing adsorbents reported previously. The cerium-doped alpha nickel hydroxide sample reported here exhibits a DAC capacity of 1.25 mmol/g that remains unaltered over 5 consecutive temperature swing adsorption−desorption cycles in the presence of oxygen and steam, successfully manifesting the high degree of hydrothermal and oxidative stability expected of sorbent formulations that are purely inorganic in composition. This study—the first one, to the best of our knowledge, to report robust, water-tolerant DAC performance at close to room temperatures for a sorbent that is purely inorganic in composition—demonstrates the potential for circumventing the use of expensive,

https://doi.org/10.1021/jacsau.4c01083
JACS Au 2025, 5, 1649−1662

hydrothermally and oxidatively unstable organic components for DAC processes currently constrained by prohibitively high sorbent costs.

4. EXPERIMENTAL SECTION

4.1. Synthesis of Porous α-Ni(OH)$_2$, α-NiCe$_{0.1}$(OH)$_x$, and α-NiFe$_{0.2}$(OH)$_x$

Porous α-Ni(OH)$_2$ was synthesized using a coprecipitation method adapted from a procedure for NiTi-LDH synthesis reported previously by the O'Hare group.[33] In a typical synthesis, 7.29 g of Ni(NO$_3$)$_2$·6H$_2$O (Thermo Scientific, 98%) were dissolved into 20 mL DI water to yield solution A, 0.6625 g of Na$_2$CO$_3$ (Alfa Aesar, >99.5%) were dissolved into 50 mL DI water to yield solution B, and 4 g of NaOH (Thermo Scientific, >97%) were dissolved into 25 mL DI water to yield solution C. The metal precursor solution A was then added dropwise into solution B under stirring, with precipitates forming almost instantaneously. Solution pH during precipitation was monitored using a pH meter (P200, Environmental Express) and was maintained within the 9−10 range by adding solution C. The resulting slurry was stirred for an additional 15 h at room temperature, followed by filtering and washing twice with 200 mL DI water and once using 100 mL ethanol. The sample not subjected to AMOST treatment—α-NiCe$_{0.1}$(OH)$_x$-no AMOST—was obtained by drying the obtained washed slurry overnight under vacuum at room temperature. In the case of samples subjected to AMOST treatment, the obtained wet solid products were dispersed into 500 mL ethanol and stirred for 6 h. The final α-Ni(OH)$_2$ product was obtained after filtering and washing with 100 mL of ethanol and drying overnight under vacuum at room temperature. The same synthesis methods were used to obtain α-NiCe$_{0.1}$(OH)$_x$ and α-NiFe$_{0.2}$(OH)$_x$ samples by adding appropriate amounts of Ce(NO$_3$)$_3$·6H$_2$O (Acros Organics, 99.5%) or Fe(NO$_3$)$_3$·9H$_2$O (Alfa Aesar, 98−101.0%), respectively, into the metal precursor solution. The subscripts 0.1 and 0.2 represent the target mole fraction of Ce or Fe of the total metal present in the sample. The synthesis procedures of other materials used in this work are described in detail in the Supporting Information.

4.2. Materials Characterization

Powder X-ray diffraction (PXRD), X-ray photoelectron spectroscopy (XPS), transmission electron microscopy (TEM), nitrogen adsorption−desorption isotherms, water vapor adsorption isotherms, Fourier transform infrared spectroscopy (FTIR), and CO$_2$ adsorption microcalorimetry were performed to evaluate the physical and chemical properties of materials. The detailed experimental procedures for these experiments are described in the Supporting Information.

4.3. CO$_2$ Adsorption Measurements

A fixed-bed adsorption setup with a mass spectrometer (Cirrus-2, MKS) downstream of the sorbent bed was used to obtain breakthrough data. A schematic for the setup is shown in Figure S15. All adsorption capacities reported are equilibrium adsorption capacities, unless specified otherwise. In a typical measurement, 0.05 g of sample was loaded into a quartz tube (4 mm inner diameter) supported by a piece of quartz wool. Prior to each breakthrough measurement, the sample was thermally activated at 200 °C under a 50 mL min^{-1} argon flow for 2 h to remove preadsorbed impurities (water, CO$_2$, and ethanol), after which the furnace was cooled down to 25 °C. The breakthrough measurement was initiated by switching the gas flow from an inert gas stream to a 50 mL min^{-1} stream of 400 ppm CO$_2$ in nitrogen (N$_2$) (Matheson, ultragrade). The experiment was terminated when the outlet CO$_2$ concentration reached 97% of the value of the inlet stream, and the corresponding adsorption capacity was calculated by integrating the area between the N$_2$ and CO$_2$ signals. A syringe pump (KD Scientific, model 100) was used to introduce water vapor into the feed stream to closely simulate ambient air. For cyclic tests, the bed was regenerated by switching the gas flow from simulated air (400 ppm of CO$_2$, balance N$_2$ at 50 mL min^{-1}) to an inert purge gas (20.2 kPa O$_2$, 2.1 kPa H$_2$O, balance Ar at 50 mL min^{-1}) at 25 °C, followed by ramping the furnace to the desired desorption temperature at a ramp rate of 10 °C/min and maintaining constant temperature for 2 h. The furnace was then cooled to 25 °C for the next adsorption cycle.

■ ASSOCIATED CONTENT

Supporting Information

The Supporting Information is available free of charge at https://pubs.acs.org/doi/10.1021/jacsau.4c01083.

Detailed experimental procedures, XRD patterns, N$_2$ physisorption isotherms, FTIR spectra, water vapor adsorption isotherms, XPS spectra, breakthrough experiment data, TEM images, schematic of fixed-bed reactor setup, and tabulated literature data (PDF)

■ AUTHOR INFORMATION

Corresponding Author

Praveen Bollini − *William A. Brookshire Department of Chemical and Biomolecular Engineering, University of Houston, Houston, Texas 77204, United States;* orcid.org/0000-0001-8092-8092; Email: ppbollini@uh.edu

Authors

Xiaowei Wu − *William A. Brookshire Department of Chemical and Biomolecular Engineering, University of Houston, Houston, Texas 77204, United States*

Rahul Pandey − *SRI International, Palo Alto, California 94304, United States;* orcid.org/0009-0006-6629-7320

Junyan Zhang − *Chemical Sciences Division, Oak Ridge National Laboratory, Oak Ridge, Tennessee 37831, United States*

Felipe Polo-Garzon − *Chemical Sciences Division, Oak Ridge National Laboratory, Oak Ridge, Tennessee 37831, United States;* orcid.org/0000-0002-6507-6183

Fransisco Carlos Robles Hernandez − *College of Engineering, Technology Division, University of Houston, Houston, Texas 77204, United States*

Ramanan Krishnamoorti − *William A. Brookshire Department of Chemical and Biomolecular Engineering, University of Houston, Houston, Texas 77204, United States;* orcid.org/0000-0001-5831-502X

Complete contact information is available at: https://pubs.acs.org/10.1021/jacsau.4c01083

Notes

Portions of the work described this manuscript have been filed as International Patent Application No. PCT/US2024/050806.

The authors declare no competing financial interest.

■ ACKNOWLEDGMENTS

The work done by J.Z. and F.P-G. was sponsored by the U.S. Department of Energy, Office of Science, Office of Basic Energy Sciences, Chemical Sciences, Geosciences, and Biosciences Division, Catalysis Science Program. F.C.R.H. wishes to thank the Welch Foundation for the grant V-E-0001. P.B. and R.K. acknowledge support from the Center for Carbon Management in Energy at the University of Houston. P.B. acknowledges support from the Department of Energy (DE-SC0025264).

REFERENCES

(1) National Academies of Sciences, Engineering and Medicine. *Negative Emissions Technologies and Reliable Sequestration: A Research Agenda*; The National Academies Press: Washington, DC, 2019.

(2) Erans, M.; Sanz-Pérez, E. S.; Hanak, D. P.; Clulow, Z.; Reiner, D. M.; Mutch, G. A. Direct Air Capture: Process Technology, Techno-Economic and Socio-Political Challenges. *Energy Environ. Sci.* **2022**, *15* (4), 1360−1405.

(3) Damm, D. L.; Fedorov, A. G. Conceptual Study of Distributed CO_2 Capture and the Sustainable Carbon Economy. *Energy Convers. Manage.* **2008**, *49* (6), 1674−1683.

(4) Lively, R. P.; Realff, M. J. On Thermodynamic Separation Efficiency: Adsorption Processes. *AIChE J.* **2016**, *62* (10), 3699−3705.

(5) Fu, D.; Park, Y.; Davis, M. E. Zinc Containing Small-Pore Zeolites for Capture of Low Concentration Carbon Dioxide. *Angew. Chem. Int. Ed.* **2022**, *61* (5), No. e202112916.

(6) Kumar, A.; Madden, D. G.; Lusi, M.; Chen, K. J.; Daniels, E. A.; Curtin, T.; Perry, J. J.; Zaworotko, M. J. Direct Air Capture of CO_2 by Physisorbent Materials. *Angew. Chem. Int. Ed.* **2015**, *54* (48), 14372−14377.

(7) Bose, S.; Sengupta, D.; Rayder, T. M.; Wang, X.; Kirlikovali, K. O.; Sekizkardes, A. K.; Islamoglu, T.; Farha, O. K. Challenges and Opportunities: Metal−Organic Frameworks for Direct Air Capture. *Adv. Funct. Mater* **2023**, *34* (43), 2307478.

(8) Wilson, S. M. W.; Tezel, F. H. Direct Dry Air Capture of CO_2 Using VTSA with Faujasite Zeolites. *Ind. Eng. Chem. Res.* **2020**, *59* (18), 8783−8794.

(9) Mukherjee, S.; Sikdar, N.; O'Nolan, D.; Franz, D. M.; Gascón, V.; Kumar, A.; Kumar, N.; Scott, H. S.; Madden, D. G.; Kruger, P. E.; et al. Trace CO_2 Capture by an Ultramicroporous Physisorbent with Low Water Affinity. *Sci. Adv.* **2019**, *5* (11), 9171−9200.

(10) Bollini, P.; Choi, S.; Drese, J. H.; Jones, C. W. Oxidative Degradation of Aminosilica Adsorbents Relevant to Postcombustion CO_2 Capture. *Energy Fuels* **2011**, *25* (5), 2416−2425.

(11) Choi, W.; Min, K.; Kim, C.; Ko, Y. S.; Jeon, J. W.; Seo, H.; Park, Y. -K.; Choi, M. Epoxide-Functionalization of Polyethyleneimine for Synthesis of Stable Carbon Dioxide Adsorbent in Temperature Swing Adsorption. *Nat. Commun.* **2016**, *7* (1), 12640.

(12) Pang, S. H.; Lee, L. C.; Sakwa-Novak, M. A.; Lively, R. P.; Jones, C. W. Design of Aminopolymer Structure to Enhance Performance and Stability of CO_2 Sorbents: Poly(Propylenimine) vs Poly(Ethylenimine). *J. Am. Chem. Soc.* **2017**, *139* (10), 3627−3630.

(13) Pang, S. H.; Lively, R. P.; Jones, C. W. Oxidatively-Stable Linear Poly(Propylenimine)-Containing Adsorbents for CO_2 Capture from Ultradilute Streams. *ChemSuschem* **2018**, *11* (15), 2628−2637.

(14) Naeem, M. A.; Armutlulu, A.; Imtiaz, Q.; Donat, F.; Schäublin, R.; Kierzkowska, A.; Müller, C. R. Optimization of the Structural Characteristics of CaO and Its Effective Stabilization Yield High-Capacity CO_2 Sorbents. *Nat. Commun.* **2018**, *9* (1), 2408.

(15) Donat, F.; Müller, C. R. Prospects of MgO-Based Sorbents for CO_2 Capture Applications at High Temperatures. *Curr. Opin. Green Sustainable Chem.* **2022**, *36*, 100645.

(16) Hiremath, V.; Kwon, H. J.; Jung, I. S.; Kwon, S.; Kwon, S. H.; Lee, S. G.; Lee, H. C.; Seo, J. G. Mg-Ion Inversion in MgO@MgO−Al2O3 Oxides: The Origin of Basic Sites. *ChemSuschem* **2019**, *12* (12), 2810−2818.

(17) Nikulshina, V.; Hirsch, D.; Mazzotti, M.; Steinfeld, A. CO_2 Capture from Air and Co-Production of H_2 via the $Ca(OH)_2$-$CaCO_3$ Cycle Using Concentrated Solar Power-Thermodynamic Analysis. *Energy* **2006**, *31* (12), 1715−1725.

(18) Rausis, K.; Stubbs, A. R.; Power, I. M.; Paulo, C. Rates of Atmospheric CO_2 Capture Using Magnesium Oxide Powder. *Int. J. Greenhouse Gas Control* **2022**, *119*, 103701.

(19) Nikulshina, V.; Gálvez, M. E.; Steinfeld, A. Kinetic Analysis of the Carbonation Reactions for the Capture of CO_2 from Air via the $Ca(OH)_2$-$CaCO_3$-CaO Solar Thermochemical Cycle. *Chem. Eng. J.* **2007**, *129* (1−3), 75−83.

(20) Dong, H.; Li, L.; Li, C. Controlled Alkali Etching of MOFs with Secondary Building Units for Low-Concentration CO_2 Capture. *Chem. Sci.* **2023**, *14*, 8507−8513.

(21) Bien, C. E.; Chen, K. K.; Chien, S. C.; Reiner, B. R.; Lin, L. C.; Wade, C. R.; Ho, W. S. W. Bioinspired Metal-Organic Framework for Trace CO_2 Capture. *J. Am. Chem. Soc.* **2018**, *140* (40), 12662−12666.

(22) Cai, Z.; Bien, C. E.; Liu, Q.; Wade, C. R. Insights into CO_2 Adsorption in M-OH Functionalized MOFs. *Chem. Mater.* **2020**, *32* (10), 4257−4264.

(23) Zhao, X.; Ning, Q.; Grabow, L. C.; Rimer, J. D.; Bollini, P. Carbonate Dimorphism, and the Reinterpretation of Rates of Lattice and Excess Oxygen-Driven Catalytic Cycles. *J. Catal.* **2022**, *416*, 423−438.

(24) Walia, S.; Balendhran, S.; Nili, H.; Zhuiykov, S.; Rosengarten, G.; Wang, Q. H.; Bhaskaran, M.; Sriram, S.; Strano, M. S.; Kalantar-Zadeh, K. Transition Metal Oxides-Thermoelectric Properties. *Prog. Mater. Sci.* **2013**, *58* (8), 1443−1489.

(25) Wang, Q.; Ohare, D. Recent Advances in the Synthesis and Application of Layered Double Hydroxide (LDH) Nanosheets. *Chem. Rev.* **2012**, *112* (7), 4124−4155.

(26) Wang, Q.; O'hare, D. Large-Scale Synthesis of Highly Dispersed Layered Double Hydroxide Powders Containing Delaminated Single Layer Nanosheets. *Chem. Commun.* **2013**, *49* (56), 6301−6303.

(27) Zick, M. E.; Pugh, S. M.; Lee, J.; Forse, A. C.; Milner, P. J. Carbon Dioxide Capture at Nucleophilic Hydroxide Sites in Oxidation-Resistant Cyclodextrin-Based Metal−Organic Frameworks. *Angew. Chem., Int. Ed.* **2022**, *61* (30), No. e202206718.

(28) Hall, D. S.; Lockwood, D. J.; Bock, C.; MacDougall, B. R. Nickel Hydroxides and Related Materials: A Review of Their Structures, Synthesis and Properties. *Proc. R. Soc. A: Math. Phys. Eng. Sci.* **2015**, *471*, 2174.

(29) Yao, J.; Li, Y.; Huang, R.; Jiang, J.; Xiao, S.; Yang, J. Crucial Role of Water Content on the Electrochemical Performance of α-$Ni(OH)_2$ as an Anode Material for Lithium-Ion Batteries. *Ionics* **2021**, *27* (1), 65−74.

(30) Shi, J.; Wu, E. A Fast and Facile Synthesis of Mesoporous Nickel Oxide. *Microporous Mesoporous Mater.* **2013**, *168*, 188−194.

(31) Li, M.; Tumuluri, U.; Wu, Z.; Dai, S. Effect of Dopants on the Adsorption of Carbon Dioxide on Ceria Surfaces. *ChemSuschem* **2015**, *8* (21), 3651−3660.

(32) Chen, C.; Wangriya, A.; Buffet, J. C.; O'Hare, D. Tuneable Ultra High Specific Surface Area Mg/Al-CO_3 Layered Double Hydroxides. *Dalton Trans.* **2015**, *44* (37), 16392−16398.

(33) Pastor, A.; Chen, C.; de Miguel, G.; Martin, F.; Cruz-Yusta, M.; Buffet, J. C.; O'Hare, D.; Pavlovic, I.; Sánchez, L. Aqueous Miscible Organic Solvent Treated NiTi Layered Double Hydroxide De-NO_x Photocatalysts. *Chem. Eng. J.* **2022**, *429*, 132361.

(34) Zhang, Z.; Huo, H.; Wang, L.; Lou, S.; Xiang, L.; Xie, B.; Wang, Q.; Du, C.; Wang, J.; Yin, G. Stacking Fault Disorder Induced by Mn Doping in $Ni(OH)_2$ for Supercapacitor Electrodes. *Chem. Eng. J.* **2021**, *412*, 128617.

(35) Metiu, H.; Chrétien, S.; Hu, Z.; Li, B.; Sun, X. Chemistry of Lewis Acid-Base Pairs on Oxide Surfaces. *J. Phys. Chem. C* **2012**, *116* (19), 10439−10450.

(36) McFarland, E. W.; Metiu, H. Catalysis by Doped Oxides. *Chem. Rev.* **2013**, *113* (6), 4391−4427.

(37) Liu, Z.; Ma, R.; Osada, M.; Iyi, N.; Ebina, Y.; Takada, K.; Sasaki, T. Synthesis, Anion Exchange, and Delamination of Co-Al Layered Double Hydroxide: Assembly of the Exfoliated Nanosheet/Polyanion Composite Films and Magneto-Optical Studies. *J. Am. Chem. Soc.* **2006**, *128* (14), 4872−4880.

(38) Sanati, S.; Rezvani, Z. Ultrasound-Assisted Synthesis of NiFe-Layered Double Hydroxides as Efficient Electrode Materials in Supercapacitors. *Ultrason. Sonochem.* **2018**, *48*, 199−206.

(39) Zhu, X.; Chen, C.; Suo, H.; Wang, Q.; Shi, Y.; O'Hare, D.; Cai, N. Synthesis of Elevated Temperature CO_2 Adsorbents from Aqueous Miscible Organic-Layered Double Hydroxides. *Energy* **2019**, *167*, 960−969.

https://doi.org/10.1021/jacsau.4c01083
JACS Au 2025, 5, 1649−1662

(40) Shang, S.; Hanif, A.; Sun, M.; Tian, Y.; Ok, Y. S.; Yu, I. K. M.; Tsang, D. C. W.; Gu, Q.; Shang, J. Novel M (Mg/Ni/Cu)-Al-CO_3 Layered Double Hydroxides Synthesized by Aqueous Miscible Organic Solvent Treatment (AMOST) Method for CO_2 Capture. *J. Hazard. Mater.* **2019**, *373*, 285−293.
(41) Wang, Y.; Wang, G.; Zhang, L.; Jin, Z.; Zhao, T. Hydroxides $Ni(OH)_2$&$Ce(OH)_3$ as a Novel Hole Storage Layer for Enhanced Photocatalytic Hydrogen Evolution. *Dalton Trans.* **2019**, *48* (47), 17660−17672.
(42) Thommes, M.; Kaneko, K.; Neimark, A. V.; Olivier, J. P.; Rodriguez-Reinoso, F.; Rouquerol, J.; Sing, K. S. W. Physisorption of Gases, with Special Reference to the Evaluation of Surface Area and Pore Size Distribution (IUPAC Technical Report). *Pure Appl. Chem.* **2015**, *87* (9−10), 1051−1069.
(43) Iyi, N.; Sasaki, T. Decarbonation of MgAl-LDHs (Layered Double Hydroxides) Using Acetate−Buffer/NaCl Mixed Solution. *J. Colloid Interface Sci.* **2008**, *322* (1), 237−245.
(44) Liu, M.; Min, K. -A.; Han, B.; Lee, L. Y. S. Interfacing or Doping? Role of Ce in Highly Promoted Water Oxidation of NiFe-Layered Double Hydroxide. *Adv. Energy Mater.* **2021**, *11* (33), 1−11.
(45) Zhang, B.; Duan, Y.; Johnson, K. Density Functional Theory Study of CO_2 Capture with Transition Metal Oxides and Hydroxides. *J. Chem. Phys.* **2012**, *136* (6), 064516.
(46) Veselovskaya, J. V.; Derevschikov, V. S.; Kardash, T. Y.; Stonkus, O. A.; Trubitsina, T. A.; Okunev, A. G. Direct CO_2 Capture from Ambient Air Using K_2CO_3/Al_2O_3 Composite Sorbent. *Int. J. Greenhouse. Gas Control* **2013**, *17*, 332−340.
(47) Masoud, N.; Clement, V.; Van Haasterecht, T.; Führer, M.; Hofmann, J. P.; Bitter, J. H. Shedding Light on Solid Sorbents: Evaluation of Supported Potassium Carbonate Particle Size and Its Effect on CO_2 Capture from Air. *Ind. Eng. Chem. Res.* **2022**, *61* (38), 14211−14221.
(48) Masoud, N.; Bordanaba-Florit, G.; Van Haasterecht, T.; Bitter, J. H. Effect of Support Surface Properties on CO_2 Capture from Air by Carbon-Supported Potassium Carbonate. *Ind. Eng. Chem. Res.* **2021**, *60* (38), 13749−13755.
(49) Zhang, H.; Wen, X.; Wang, Y. Synthesis and Characterization of Sulfate and Dodecylbenzenesulfonate Intercalated Zinc−Iron Layered Double Hydroxides by One-Step Coprecipitation Route. *J. Solid State Chem.* **2007**, *180* (5), 1636−1647.
(50) Wang, X.; Zhao, H.; Chang, L.; Yu, Z.; Xiao, Z.; Tang, S.; Huang, C.; Fan, J.; Yang, S. First-Principles Study on Interlayer Spacing and Structure Stability of NiAl-Layered Double Hydroxides. *ACS Omega* **2022**, *7* (43), 39169−39180.
(51) Chen, H.; Dong, H.; Shi, Z.; SenGupta, A. K. Direct Air Capture (DAC) and Sequestration of CO_2: Dramatic Effect of Coordinated Cu(II) onto a Chelating Weak Base Ion Exchanger. *Sci. Adv.* **2023**, *9* (10), No. eadg1956.
(52) Coenen, K.; Gallucci, F.; Mezari, B.; Hensen, E.; van Sint Annaland, M. An In-Situ IR Study on the Adsorption of CO_2 and H_2O on Hydrotalcites. *J. CO2 Util.* **2018**, *24*, 228−239.
(53) Yoshikawa, K.; Sato, H.; Kaneeda, M.; Kondo, J. N. Synthesis and Analysis of CO_2 Adsorbents Based on Cerium Oxide. *J. CO2 Util.* **2014**, *8*, 34−38.
(54) Rudolph, W. W.; Fischer, D.; Irmer, G. Vibrational Spectroscopic Studies and Density Functional Theory Calculations of Speciation in the CO_2—Water System. *Appl. Spectrosc.* **2006**, *60* (2), 130−144.
(55) Shi, X.; Xiao, H.; Chen, X.; Lackner, K. S. The Effect of Moisture on the Hydrolysis of Basic Salts. *Chem. - A Eur. J.* **2016**, *22* (51), 18326−18330.
(56) Gankanda, A.; Cwiertny, D. M.; Grassian, V. H. Role of Atmospheric CO_2 and H_2O Adsorption on ZnO and CuO Nanoparticle Aging: Formation of New Surface Phases and the Impact on Nanoparticle Dissolution. *J. Phys. Chem. C* **2016**, *120* (34), 19195−19203.
(57) Shi, X.; Xiao, H.; Kanamori, K.; Yonezu, A.; Lackner, K. S.; Chen, X. Moisture-Driven CO_2 Sorbents. *Joule* **2020**, *4* (8), 1823−1837.
(58) Shi, X.; Xiao, H.; Lackner, K. S.; Chen, X. Capture CO_2 from Ambient Air Using Nanoconfined Ion Hydration. *Angew. Chem., Int. Ed.* **2016**, *55* (12), 4026−4029.
(59) Shi, X.; Xiao, H.; Azarabadi, H.; Song, J.; Wu, X.; Chen, X.; Lackner, K. S. Sorbents for the Direct Capture of CO_2 from Ambient Air. *Angew. Chem., Int. Ed.* **2020**, *59* (18), 6984−7006.
(60) Wang, T.; Lackner, K. S.; Wright, A. Moisture Swing Sorbent for Carbon Dioxide Capture from Ambient Air. *Environ. Sci. Technol.* **2011**, *45* (15), 6670−6675.
(61) Azarabadi, H.; Lackner, K. S. A Sorbent-Focused Techno-Economic Analysis of Direct Air Capture. *Appl. Energy.* **2019**, *250*, 959−975.
(62) Kumar, R.; Ohtani, S.; Tsunoji, N. Direct Air Capture on Amine-Impregnated FAU Zeolites: Exploring for High Adsorption Capacity and Low-Temperature Regeneration. *Microporous Mesoporous Mater.* **2023**, *360*, 112714.
(63) He, Z.; Wang, Y.; Miao, Y.; Wang, H.; Zhu, X.; Li, J. Mixed Polyamines Promotes CO_2 adsorption from Air. *J. Environ. Chem. Eng.* **2022**, *10* (2), 107239.
(64) Wadi, B.; Golmakani, A.; Manovic, V.; Nabavi, S. A. Evaluation of Moderately Grafted Primary, Diamine, and Triamine Sorbents for CO_2 Adsorption from Ambient Air: Balancing Kinetics and Capacity under Humid Conditions. *Ind. Eng. Chem. Res.* **2021**, *60* (36), 13309−13317.
(65) Wang, W.; Liu, F.; Zhang, Q.; Yu, G.; Deng, S. Efficient Removal of CO_2 from Indoor Air Using a Polyethyleneimine-Impregnated Resin and Its Low-Temperature Regeneration. *Chem. Eng. J.* **2020**, *399*, 125734.
(66) Meng, Y.; Jiang, J.; Aihemaiti, A.; Ju, T.; Gao, Y.; Liu, J.; Han, S. Feasibility of CO_2 Capture from O_2-Containing Flue Gas Using a Poly(ethylenimine)-Functionalized Sorbent: Oxidative Stability in Long-Term Operation. *ACS Appl. Mater. Interfaces* **2019**, *11* (37), 33781−33791.
(67) Gebald, C.; Wurzbacher, J. A.; Tingaut, P.; Steinfeld, A. Stability of Amine-Functionalized Cellulose during Temperature-Vacuum-Swing Cycling for CO_2 Capture from Air. *Environ. Sci. Technol.* **2013**, *47* (17), 10063−10070.
(68) Carneiro, J. S. A.; Innocenti, G.; Moon, H. J.; Guta, Y.; Proaño, L.; Sievers, C.; Sakwa-Novak, M. A.; Ping, E. W.; Jones, C. W. Insights into the Oxidative Degradation Mechanism of Solid Amine Sorbents for CO_2 Capture from Air: Roles of Atmospheric Water. *Angew. Chem., Int. Ed.* **2023**, *62* (24), No. e202302887.
(69) Sujan, A. R.; Pang, S. H.; Zhu, G.; Jones, C. W.; Lively, R. P. Direct CO_2 Capture from Air Using Poly(ethylenimine)-Loaded Polymer/Silica Fiber Sorbents. *ACS Sustainable Chem. Eng.* **2019**, *7* (5), 5264−5273.
(70) Miao, Y.; He, Z.; Zhu, X.; Izikowitz, D.; Li, J. Operating Temperatures Affect Direct Air Capture of CO_2 in Polyamine-Loaded Mesoporous Silica. *Chem. Eng. J.* **2021**, *426*, 131875.
(71) Sujan, A. R.; Kumar, D. R.; Sakwa-Novak, M.; Ping, E. W.; Hu, B.; Park, S. J.; Jones, C. W. Poly(glycidyl amine)-Loaded SBA-15 Sorbents for CO_2 Capture from Dilute and Ultradilute Gas Mixtures. *ACS Appl. Polym. Mater.* **2019**, *1* (11), 3137−3147.
(72) Bhatt, P. M.; Belmabkhout, Y.; Cadiau, A.; Adil, K.; Shekhah, O.; Shkurenko, A.; Barbour, L. J.; Eddaoudi, M. A Fine-Tuned Fluorinated MOF Addresses the Needs for Trace CO_2 Removal and Air Capture Using Physisorption. *J. Am. Chem. Soc.* **2016**, *138* (29), 9301−9307.
(73) Wilson, S. M. W. High Purity CO_2 from Direct Air Capture Using a Single TVSA Cycle with Na-X Zeolites. *Sep. Purif. Technol.* **2022**, *294*, 121186.

https://doi.org/10.1021/jacsau.4c01083
JACS Au 2025, 5, 1649−1662